CrossMark

Acetohydroxamic acid adsorbed at copper surface: electrochemical, Raman and theoretical observations

Juan Du[1] · Ye Ying[1] · Xiao-yu Guo[1] · Chuan-chuan Li[1] · Yiping Wu[1] · Ying Wen[1] · Hai-Feng Yang[1]

Abstract Corrosion inhibition effect of AHA film formed on the copper surface by self-assembled monolayers technique was estimated in 3 wt% NaCl solution by electrochemical impedance spectroscopy and polarization methods. Polarization data indicated that AHA was an anodic inhibitor. The maximum inhibition efficiency reached 93.5% in the case of assembly 3 h in 10 mM AHA solution. The adsorption of AHA on the copper surface fits Langmuir adsorption isotherm. Surface-enhanced Raman scattering together with quantum chemical studies demonstrated that N–O and C=O groups were attached to the copper surface, predicting the feasible adsorption centers and confirming the relationship between the molecular structures of AHA and its inhibition property.

Keywords Acetohydroxamic acid · EIS · Polarization · SERS · Anodic inhibitor

Introduction

Highly electrical and thermal conductivities, as well as good mechanical workability of copper and its alloys enable them to have a diverse range of applications in pipelines for domestic and industrial water systems, ship-building, seawater desalination and heat exchanger [1–5].

However, copper and its alloys suffer serious corrosion in chloride environments, causing huge economy losses [6–8]. Thus, a considerable amount of efforts have been made to improve the corrosion resistance properties of copper using effective organic inhibitors with aromatic rings, and electronegative functional groups involving the heteroatoms of sulfur, nitrogen and oxygen, which may adsorb at the copper surface to form inhibitive coatings [9–15].

Unfortunately, among them, some are toxic and expensive. In recent years, various types of nontoxic organic compounds have been investigated to meet the recommendation using eco-friendly inhibitors as substitutes for restricted toxic inhibitors [16–21]. Some hydroxamic acids and their derivatives with biological activities, such as anti-inflammatory and anti-asthmatic, are used as pesticides and plant growth promoters [22]. In addition, hydroxamic acids could chelate with metal ions to form complexes [23, 24]. Thus, hydroxamic acid derivatives have already been reported as effective corrosion inhibitors for carbon steel and copper corrosion [25–27]. AHA as a potential corrosion inhibitor could form a protection film on the copper surface due to multiple adsorption centers of a nitrogen atom and two oxygen atoms in its structure (see Scheme 1). So far, the adsorption behavior of AHA on copper surface as well as its corrosion inhibition efficiency has not been observed in detail.

In this work, AHA was adsorbed on copper surface by self-assembled monolayers (SAMs) technique and the efficiency against corrosion in 3 wt% NaCl solution was estimated by electrochemical impedance spectroscopy (EIS) and polarization methods. SERS technique as a powerful tool to provide molecular fingerprint information was used to elucidate formation mechanism of AHA coating on the copper surface as well as Langmuir

✉ Ye Ying
  yingye@shnu.edu.cn

✉ Hai-Feng Yang
  haifengyang@yahoo.com

1 The Education Ministry Key Lab of Resource Chemistry, Department of Chemistry, Shanghai Normal University, Shanghai 200234, People's Republic of China
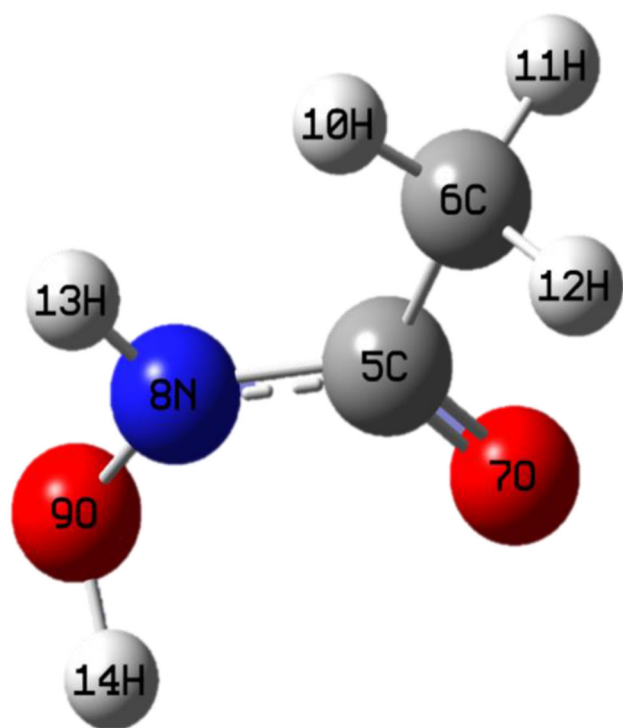
Scheme 1 Optimized structure of acetohydroxamic acid

adsorption isotherm measurement. Furthermore, quantum chemical studies were used to predict the feasible adsorption centers and confirm the relationship between the molecular structures of AHA and its inhibition property.

Experimental

Materials and chemicals

Acetohydroxamic acid (AHA) was purchased from Sigma-Aldrich. Analytical grade NaCl was dissolved in ultrapure water (18 MΩ cm) to prepare 3 wt% NaCl corrosion media. Sulfuric acid and ethanol were analytical reagents, purchased from Sinopharm Chemical Reagents Company.

Apparatus

Raman spectroscopic measurement was conducted using LabRam II confocal Laser Raman system (Dilor, France). A 1024 × 800 pixels charge-coupled device detector cooled by semiconductor was used, and the excitation source was a He–Ne laser at 632.8 nm with power of ca. 5 mW. The slit and pinhole were controlled at 100 and 1000 μm, respectively. The laser was focused onto the copper surface through a long-working-length of 50× objective. Each Raman spectrum was taken with 8 s

integration time and 3× repeats. The line of silicon positioned at 519 cm^{-1} was used for spectral calibration.

The electrochemical measurements were carried out using CHI 750C electrochemistry workstation (CH Instruments, Inc.).

Pretreatment for electrode

The copper electrode was constructed from polycrystalline copper (99.999%) rod inside of a Teflon sheath, and the exposure area of surface was 0.0314 cm^2. Before the Raman spectroscopic and electrochemical measurements, the copper electrode was sequentially abraded with 500- and 1000-grit papers, followed by 0.3 μm alumina powders to get a shiny mirror-like electrode surface, and then cleaned with Milli-Q water and pure ethanol in an ultrasonic bath to remove any remaining alumina particles and possible rust. For SERS detection, to obtain the necessary roughness of the copper surface, copper surface was first treated in 2 M H$_2$SO$_4$ solution using an oxidation–reduction cycle (ORC) process in the potential range from −0.55 to 0.45 V (vs. SCE) with scan rate at 0.02 V/s and 10 sweep segments and final potential was applied at −0.55 V (vs. SCE) for 60 s [28]. In a conventional three-electrode cell, the AHA-modified copper electrode (or bare copper specimen) and a platinum electrode were used as working electrode and the counter electrode, respectively. All potentials referred to in this paper are reported relative to the saturated calomel electrode (SCE), which was used as reference electrode.

Coating the copper surface with AHA

The cleaned copper electrodes were immersed immediately into the deoxygenated AHA solutions with various concentrations. The assembly time effect on the formation of AHA film at the Cu surface was also considered. Before spectroscopic and electrochemical experiments, the AHA solution was removed and the electrode surface with AHA film was rinsed using Milli-Q water, and then dried by flowing nitrogen gas.

Electrochemical measurements

The impedance spectra were performed in a three-electrode cell starting from open circuit potential (OCP) with the AC voltage amplitude of 5 mV (vs. SCE) in the frequency range from 0.01 Hz to 100 kHz. The impedance results were simulated with a compatible electronic equivalent circuit fitting. The electrochemical polarization curves were obtained from −0.1 V (vs. SCE) to −0.3 V (vs. SCE) with a scan rate of 1 mV s^{-1}.
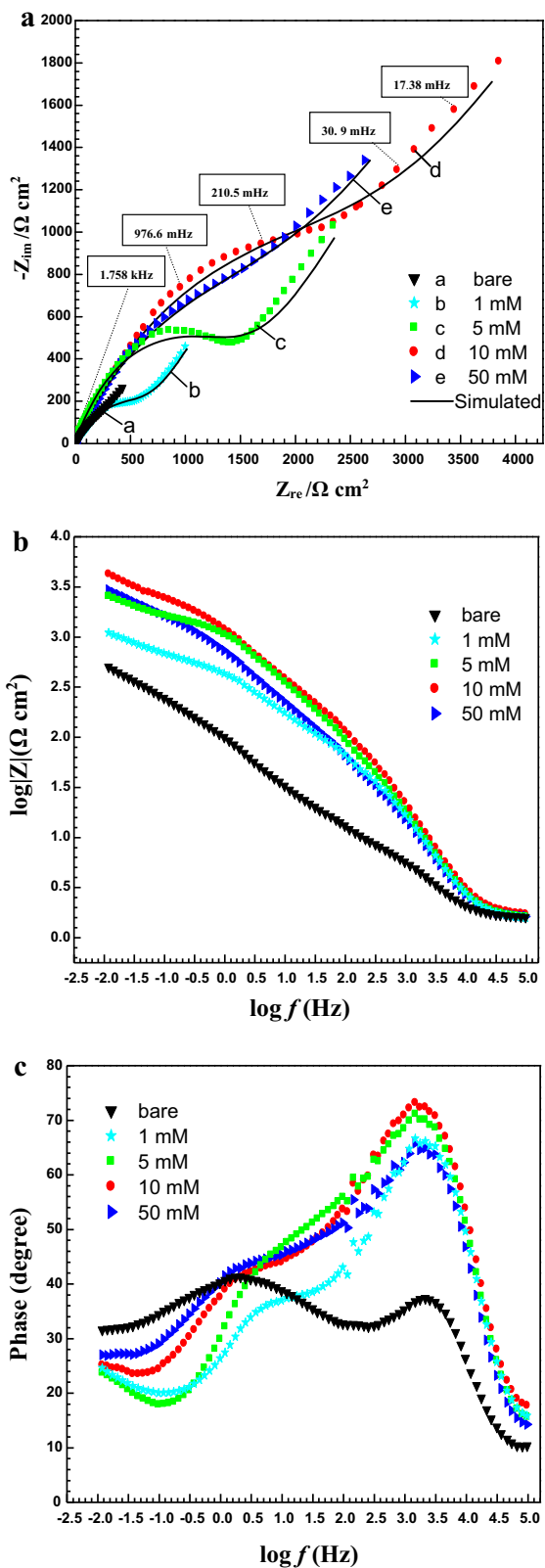
Fig. 1 Nyquist (**a**), bode (**b**) and phase angle (**c**) plots of copper electrodes with acetohydroxamic acid films formed in different concentrations of acetohydroxamic acid solutions, acquired in 3 wt% NaCl solution
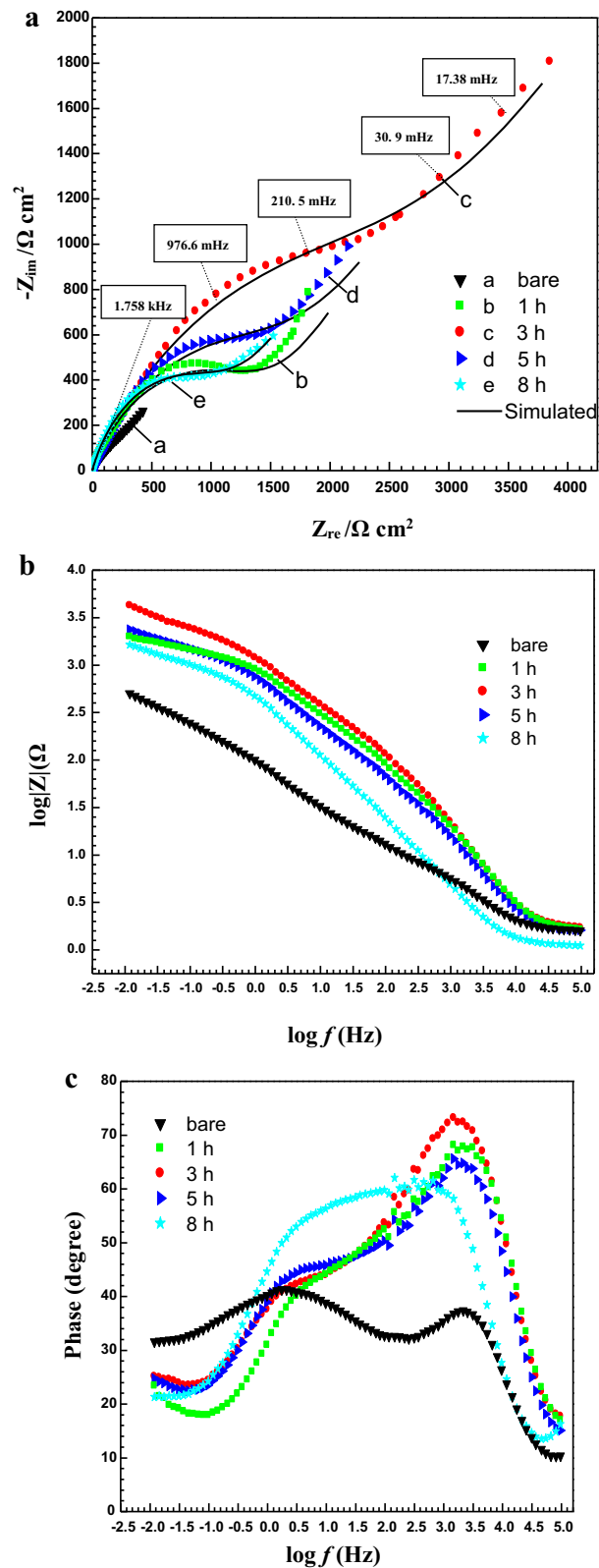
Fig. 2 Nyquist (**a**), Bode (**b**) and phase angle (**c**) plots of copper electrodes in the absence and presence of film formed in 10 mM acetohydroxamic acid solution for different time, recorded in 3 wt% NaCl solution
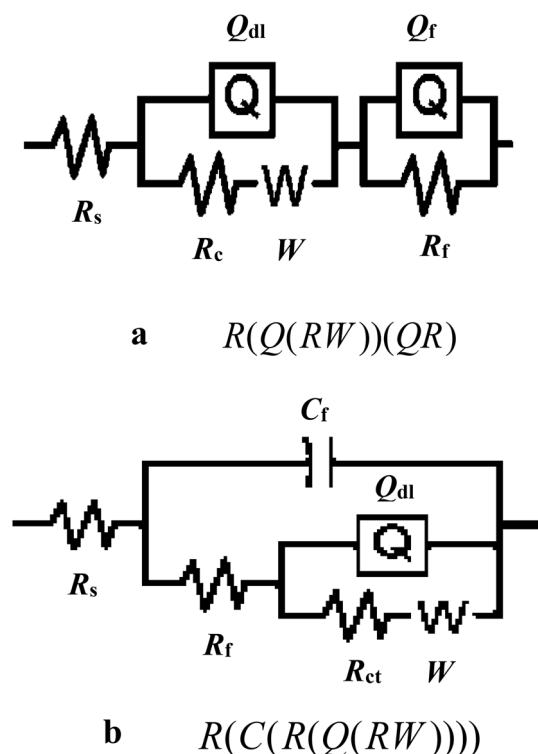
Fig. 3 The electrical equivalent circuit models for impedance data of copper electrode without film (**a**) with AHA film (**b**)

observed using GaussView 5.0. The SERS bands of AHA molecule were tentatively assigned according to the computation result obtained using B3LYP/Lanl2DZ method on the basis of AHA-Cu$_4$ mode. Additionally, the calculations of the frequencies have been scaled by a factor of 0.9940 for B3LYP/6-31G(d) level and a uniform scaling factor of 0.9762 for B3LYP/LanL2DZ method.

Results and discussion

EIS spectra

Electrochemical impedance spectroscopy for studying the inhibitor against corrosion does not result in any destruction of the film state on the electrode surface [29].

Nyquist plots along with bode and phase angle plots for the copper electrodes with AHA films formed in various AHA concentration solutions and under different assembly time corroded in 3 wt% NaCl solutions are shown in Figs. 1 and 2. The shape of the Nyquist plot for bare copper electrode is different from those of AHA-modified electrodes. The latter ones are composed of a high-frequency imperfect semicircle and a straight line seen as Warburg impedance in the low frequency [30].

Clearly, the Warburg impedance for copper is connected with the diffusion of many oxide species due to lacking protection film [31]. In Fig. 1a, compared with that of bare copper electrode, semicircle diameters of the electrodes with AHA increase visibly and it reaches a maximum when the film was formed in 10 mM AHA solution. It means that formed in an optimized assembly concentration of AHA

Theory computation details

The geometry optimization of AHA molecule and its Raman spectral calculation were performed at the density functional theory (DFT) based on B3LYP/6-31G(d) level using Gaussian 03 package and the vibrations were

Table 1 Electrochemical parameters calculated from EIS measurements for copper electrodes without the AHA films, in 3 wt% NaCl solution
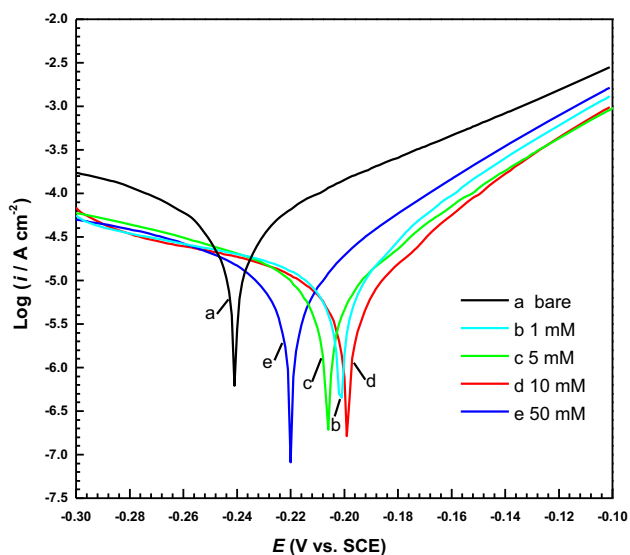
C_{AHA} (mM)	E_{OCP} (V vs. SCE)	R_s (Ω cm^2)	Q_f $Y_0 \times 10^{-3}$ (Ω^{-1} cm^{-2} s^{n1})	n_1	R_f (Ω cm^2)	Q_{dl} $Y_0 \times 10^{-4}$ (Ω^{-1} cm^{-2} s^{n2})	n_2	R_{ct} (Ω cm^2)	R_p (Ω cm^2)	W Y_0 (Ω^{-1} cm^{-2} n$^{0.5}$)	η (%)
Bare	−0.193	1.45	5.37	0.565	227	1.08	0.858	4.84	232	0.0109	–

Table 2 Electrochemical parameters calculated from EIS measurements for copper electrodes with the AHA films formed in different concentrations of AHA solutions, in 3 wt% NaCl solution

C_{AHA} (mM)	E_{OCP} (V vs. SCE)	R_s (Ω cm^2)	C_f (μF cm^{-2})	R_f (Ω cm^2)	Q_{dl} $Y_0 \times 10^{-4}$ (Ω^{-1} cm^{-2} S^n)	n	R_{ct} (Ω cm^2)	R_p (Ω cm^2)	W $Y_0 \times 10^{-3}$ (Ω^{-1} cm^{-2} S$^{0.5}$)	η (%)
1	−0.200	1.59	7.61	24.5	5.93	0.515	764	789	5.92	70.7
5	−0.225	1.62	7.24	39.0	1.77	0.611	1638	1677	2.83	86.2
10	−0.236	1.72	6.31	54.7	2.46	0.540	3489	3544	1.68	93.5
20	−0.224	1.64	8.31	32.4	3.81	0.536	1996	2028	2.21	88.6
40	−0.225	1.62	6.48	29.0	3.05	0.485	1457	1486	4.00	84.4
50	−0.230	1.62	8.07	16.2	4.36	0.536	2789	2805	2.16	91.7

Table 3 Electrochemical impedance parameters for copper electrodes in 3 wt% NaCl solution, in the absence and presence of film formed in 10 mM AHA solution for different time

Time (h)	E_{OCP} (V vs. SCE)	R_s (Ω cm^2)	C_f (μF cm^{-2})	R_f (Ω cm^2)	Q_{dl} $Y_0 \times 10^{-4}$ (Ω^{-1} cm^{-2} S^n)	n	R_{ct} (Ω cm^2)	R_p (Ω cm^2)	W $Y_0 \times 10^{-3}$ (Ω^{-1} cm^{-2} S$^{0.5}$)	η (%)
1	−0.212	1.62	5.98	26.6	2.44	0.576	1586	1613	4.18	85.6
3	−0.236	1.72	6.31	54.7	2.46	0.540	3489	3544	1.68	93.5
5	−0.222	1.61	7.68	20.9	3.66	0.569	2008	2029	3.30	88.6
8	−0.251	1.05	13.7	0.111	5.02	0.655	1270	1270	5.39	81.8

Fig. 4 Anodic and cathodic polarization curves of the copper without and with AHA film formed at different concentrations for 3 h: *a* bare, *b* 1 mM, *c* 5 mM, *d* 10 mM, *e* 50 mM, in 3 wt% NaCl solution
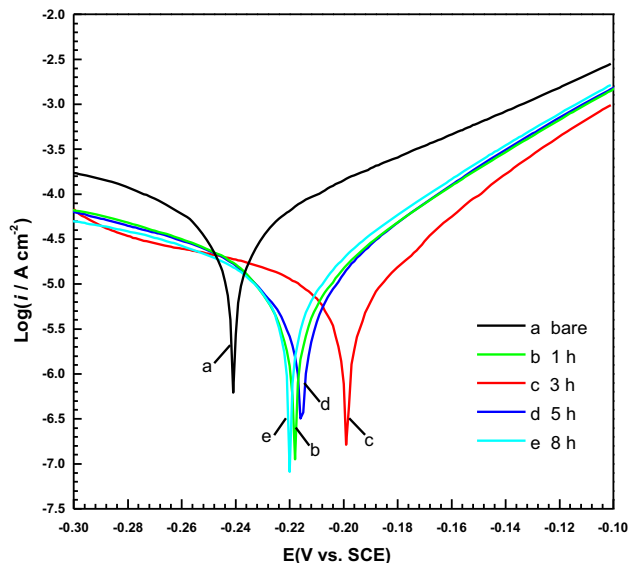
Fig. 5 Anodic and cathodic polarization curves for copper electrodes without and with AHA films formed in 10 mM AHA solution for different time: *a* bare, *b* 1 h, *c* 3 h, *d* 5 h, *e* 8 h in 3 wt% NaCl solution

solution, molecular adsorption layer on the copper surface is compact for enhancing corrosion protection [32]. Similarly, the Z_{mod} value of the bode plot (Fig. 1b) and phase angle value from phase angle plot (Fig. 1c) for the film-modified electrodes formed in 10 mM AHA solution are highest, indicating a superior protection performance. In Fig. 2a, semicircle diameter of the electrode with AHA formed in 10 mM AHA solution for 3 h assembly time comes to the greatest value; the same results have been observed in the bode plots (Fig. 2b) and phase angle plots (Fig. 2c). If the assembly time is less than 3 h, the AHA layer adsorbed on the electrode might not be dense enough while more than 3 h, accumulation of AHA molecules occurs on the surface, which also affects the compact structure of film and hinders inhibition of copper corrosion.

The equivalent circuit models for analyzing impedance characteristics of electrodes with and without AHA are displayed in Fig. 3. Such equivalent circuit models were selected, considering the possible adsorption fashion and the film structure of AHA at the copper surface as well as

evaluating the least error for each parameter routinely less than 10% and the Chi-square values (χ^2) less than 1×10^{-3}.

In Fig. 3a, the equivalent circuit model of R(Q(RW))(QR) is fitting the Nyquist plot of the bare copper while R(C(R(Q(RW)))) equivalent circuit in Fig. 3b is for the AHA-modified copper.

R_s is the solution resistance, and R_{ct}, the charge transfer resistance is attributed to the corrosion reaction at the electrode/solution interface [33]. R_f represents the resistance of the film formed on the copper surface, and W indicates the Warburg impedance. Q_{dl} and Q_f are defined as constant phase elements (CPE), representing film capacitance and a modified double-layer capacitance [34], described by the following equation [35]:

$$Z_{CPE} = Y_0^{-1}(j\omega)^{-n} \qquad (1)$$

where Y_0 is the modulus, j is the imaginary root, ω is the angular frequency and n is the phase ($-1 \leq n \leq +1$).

Table 4 Corrosion parameters obtained from potentiodynamic polarization curves for copper surface without and with AHA film formed in different concentrations of AHA solutions for 3 h assembly time, in 3 wt% NaCl solutions

C_{AHA} (mM)	E_{corr} (V vs. SCE)	i_{corr} (uA cm^{-2})	β_c (V dec^{-1})	β_a (V dec^{-1})	η (%)
Bare	−0.241	78.89	4.323	12.84	–
1	−0.201	17.25	6.748	18.21	78.13
5	−0.206	13.29	6.712	17.61	83.15
10	−0.199	10.13	9.460	19.61	87.16
50	−0.197	11.12	8.770	18.91	85.90

Table 5 Polarization parameters for the copper without and with AHA film formed in 10 mM AHA solution for different time, in 3 wt% NaCl solution

Time (h)	E_{corr} (V vs. SCE)	i_{corr} (uA cm^{-2})	β_c (v dec^{-1})	β_a (v dec^{-1})	η (%)
Bare	−0.241	78.89	4.323	12.84	–
1	−0.218	13.2	4.207	17.81	83.27
3	−0.199	10.13	9.460	19.61	87.16
5	−0.216	12.2	5.454	17.61	84.54
8	−0.220	17.09	3.055	17.71	78.34

Table 6 Comparison of the inhibition efficiencies of different copper inhibitors

Inhibitor	Concentration (mM)	Medium	η (%)	References
AHA	10	3 wt% NaCl	93.5	This work
DMTD	10	0.5 M HCl	84.3	Qin et al. [40]
PU	10	1 M NaCl	76.0	Scendo [41]
MPTT	20	0.5 M NaCl	94.4	Chen et al. [42]
BBTD	1	3 wt% NaCl	87.6	Zhang et al. [5]
AAP	10	3 wt% NaCl	90.6	Song et al. [30]

Relying on the different values of n, CPE may be inductance ($n = -1$, $Q = L$), resistance ($n = 0$, $Q = R$), Warburg impedance ($n = 0.5$, $Q = W$) or capacitance ($n = 1$, $Q = C$).

Electrochemical parameters calculated from EIS measurements for copper electrodes without and with AHA films are listed in Table 1 (bare copper), Table 2 (with films formed in different AHA concentrations solutions) and Table 3 (with films under different assembly time).

All the n values are over 0.5, indicating the relatively low corrosion of the electrode [36]. The inhibition efficiency (η%) is described in the following equation [37]:

$$\eta(\%) = \frac{R_p - R_p^0}{R_P} \times 100 \qquad (2)$$

R_p^0 refers the polarization resistance of the bare copper, and R_p is the polarization resistance of the AHA-modified electrode (R_p is the sum of R_{ct} and R_f) [38].

Observation from the three Tables reveals that the R_p values for the AHA-modified copper electrodes increase visibly and the W values tend to decrease obviously compared to the bare copper electrode. Under the above-mentioned optimized condition, R_p reaches the maximum value, W reaches the minimum value and the maximum inhibition efficiency reaches 93.5%. The RSD (relative standard deviation) of the inhibition efficiencies calculated from electrochemical impedance parameters for three copper electrodes with film is 0.13%. In all, impedance data suggest that the AHA monolayer has a remarkable protection behavior for copper.

Polarization measurements

Polarization curves of the electrodes with different AHA concentrations and different assembly time recorded in 3 wt% NaCl solutions are given in Figs. 4 and 5,
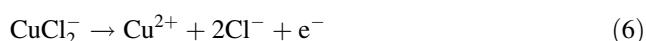
Fig. 6 Micrographs of copper surfaces with AHA film formed in 10 mM AHA solution for 3 h assembly time (**a**), and with AHA film formed in same condition as a and exposed to 3 wt% NaCl for 5 h (corrosion time) at 298 K (**b**). Bare copper before (**c**) and after (**d**) exposed to 3 wt% NaCl for 5 h (corrosion time) at 298 K
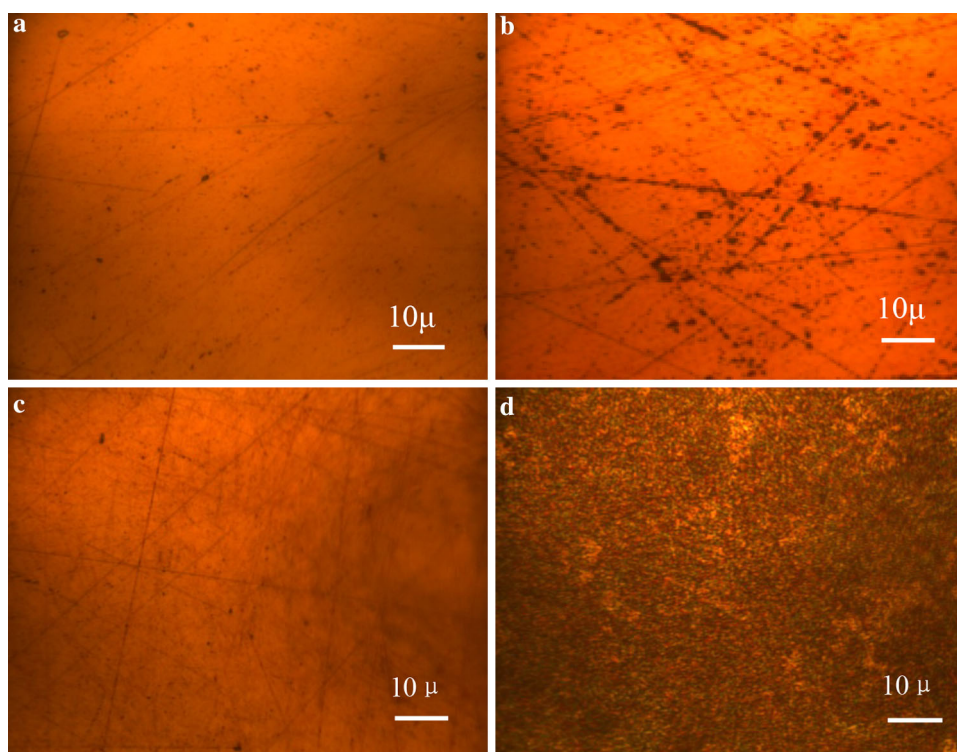
respectively. The reaction of the cathodic oxygen reduction is depicted as follows:

$$O_2 + 4e^- + 2H_2O \rightarrow 4OH^- \tag{3}$$

Also, in the presence of Cl^-, the anodic dissolution process of copper consists of the following steps (the ionization of copper with Cl^- and the diffusion of $CuCl_2^-$ to the bulk solution) [39]:

$$Cu + Cl^- \rightarrow CuCl + e^- \tag{4}$$

$$CuCl + Cl^- \rightarrow CuCl_2^- \tag{5}$$

$$CuCl_2^- \rightarrow Cu^{2+} + 2Cl^- + e^- \tag{6}$$

The related electrochemical parameters obtained from the polarization curves, such as cathodic and anodic Tafel slopes (β_c and β_a), corrosion potential (E_{corr}), corrosion current density (i_{corr}) and the inhibition efficiency ($\eta\%$), are given in Tables 4 and 5. E_{corr} and i_{corr} were estimated by the method of Tafel extrapolation.

It can be seen from Figs. 4 and 5 that the Tafel slopes greatly change after the addition of AHA. Besides, current densities shift to lower values obviously at the same potential, compared with the bare electrode. Additionally, corrosion potential shifts to the positive direction significantly, indicating that AHA has more pronounced influence in the anodic dissolution process of copper with respect to the cathodic oxygen reduction. It might point out that in Fig. 4 the plot c (5 mM) looks tricky in comparison with others. We repeated the each experiment more than 5× and the results were quite similar. A possible reason was that

the best uniform and compact film of AHA at the copper surface just formed under optimal concentration and assembly time.

The comparison of this work with other inhibitors, such as 4-amino-antipyrine (AAP) [30], as well as 2,5-dimer-capto-1,3,4-thiadiazole (DMTD) [40], bis-(1-benzotria-zolymethylene)-(2,5-thiadiazoly)-disulfide (BBTD) [5], purine (PU) [41], 5-Mercapto-3-phenyl-1,3,4-thiadiazole-2-thione potassium (MPTT) [42], is listed in Table 6. By contrast, it can be seen that the AHA is an effective corrosion inhibitor for copper in 3 wt% NaCl.

Microscopic analysis

Figure 6 shows the surface morphologies of AHA-modified copper and bare copper electrode corroded in 3 wt% NaCl solutions for 5 h. In Fig. 6d, after 5 h immersion in high-salt media, the porous structure and rough surface of the bare copper indicate serious corrosion occurrence while the corrosion behavior of the AHA-modified copper surface is less severe under the same condition (see Fig. 6b). The above observation confirms that AHA is an effective inhibitor for copper corrosion, acquired from electro-chemical measurement.

Adsorption isotherm

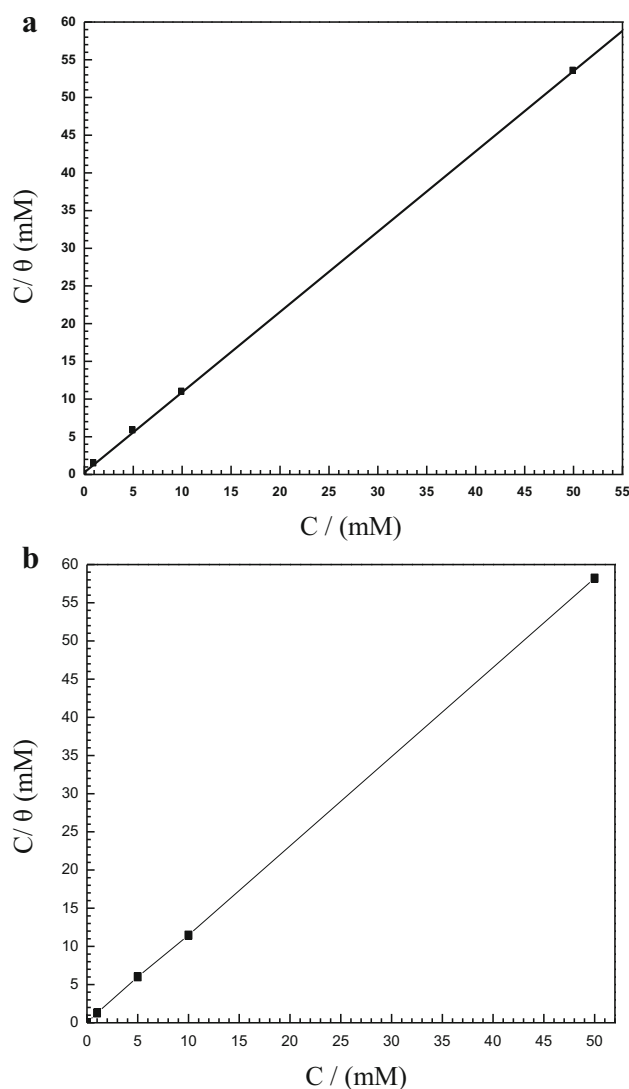For further shedding insight on adsorption mechanism of inhibitor interaction with the copper surface, many

Fig. 7 Langmuir adsorption isotherm plot for AHA film formed under the optimized condition at the copper surface in 3 wt% NaCl solution at 298 K according to **a** EIS results and **b** potentiodynamic polarization results

adsorption modes such as the Langmuir, Temkin and Frumkin isotherms could be investigated [43]. Therefore, the surface coverage (θ) for different concentrations of AHA modification film was calculated from EIS parameters in Table 1 ($\eta(\%) = 100 \times \theta$).

It is found that the adsorption of AHA on the copper surface can be described by Langmuir adsorption isotherm equation [44, 45]:

$$\frac{c}{\theta} = \frac{1}{K_{ads}} + c \tag{7}$$

where K_{ads} is the equilibrium constant, θ is the degree of surface coverage on the metal surface and c is the AHA concentration. According to EIS experimental results, a plot of c/θ against c (Fig. 7a) showed a straight line

($y = 1.06463x + 0.2659$), with the linear correlation coefficient $R^2 = 0.9999$, and its nearly unit slope confirms that the adsorption of AHA on the copper surface fits Langmuir adsorption isotherm. Additionally, adsorption isotherm drawn from potentiodynamic polarization results in Table 4 is also given in Fig. 7b. A plot of c/θ against c shows a straight line ($y = 1.16282x + 0.0452$), with the linear correlation coefficient $R^2 = 0.9999$.

In addition, the standard free energy of adsorption, ΔG_{ads}^0, is obtained from the following equation [46]:

$$\Delta G_{ads}^0 = -RT \ln(55.5 K_{ads}) \tag{8}$$

where R is the general gas constant (8.314 J mol^{-1} K^{-1}), the temperature in Kelvin (298.15 K) is the absolute temperature, and the value of 55.5 mol L^{-1} is the concentration of water in pure solution. The calculated K_{ads} values are 3.76×10^3 M^{-1} and 2.21×10^4 M^{-1}, based on EIS and potentiodynamic polarization results, respectively. The relevant ΔG_{ads}^0 is -30.4 kJ mol^{-1} (EIS results) or -34.8 kJ mol^{-1} (potentiodynamic polarization results). The large negative value of ΔG_{ads}^0 indicates that AHA was strongly adsorbed on the copper surface [47, 48].

Raman studies

Figure 8a, b illustrates the normal Raman spectrum of AHA powder and SERS spectrum of the AHA-modified copper electrode formed in 10 mM AHA solution for 3 h assembly time, respectively. Table 7 shows density functional theory (DFT) calculation results for Raman and SERS analysis. The corresponding assignments for Raman spectral analysis were performed on the basis of B3LYP/6-31G(d) calculation. Also, to assign SERS spectrum of AHA, DFT calculation for geometry optimization and vibration modes based on B3LYP/LanL2DZ was performed with model AHA-Cu$_4$ [49]. The optimized geometry model AHA-Cu$_4$ can be seen in Fig. 9.

It should be mentioned that in inset of Fig. 8 with spectral range from 200 to 750 cm^{-1}, the Raman bands around 528 and 618 cm^{-1} are from the oxide species of copper, indicating that the oxide layers were inevitably generated in ORC pretreatment process for SERS activity of copper [50].

Combined with the calculation results in Table 7, we can better understand the vibrational modes in Fig. 8a, b. In Fig. 8a, the Raman peaks at 967 and 989 cm^{-1} represent N–O–H bending in plane and C–H bending in plane. The stretching vibration modes of N–O, C–C, C=O and C–H appear at 1088, 1366, 1619 and 2998 cm^{-1}. The asymmetric stretching vibration mode of C–H appears at 2941 cm^{-1}. The Raman peaks at 1390 cm^{-1} represent OH bending and C-N bending out of plane.

Fig. 8 *a* Normal Raman spectrum of AHA in powder, *b* SERS spectrum of AHA film at the copper electrode formed in 10 mM AHA solution for 3 h assembly time, *inset* showing the SERS spectrum (200–750 cm^{-1}) of the oxide layers
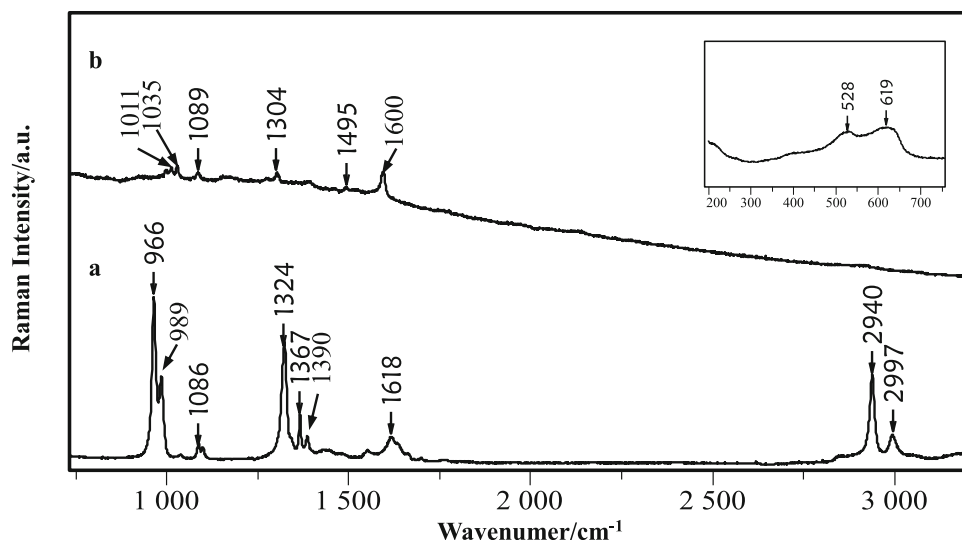

Table 7 Assignment for Raman vibrational modes of AHA and SERS vibrational modes of AHA-Cu$_4$ based on DFT calculation

Raman (cm^{-1})	Calculated Raman (cm^{-1}) (B3LYP/6-31G(d))	Approximate assignment	SERS (cm^{-1})	Calculated SERS (cm^{-1}) (AHA-Cu$_4$)	Approximate assignment
967^s	957	N–O–H$^{ip.bend}$		940	C–N–H$^{str.}$
989^s	1011	C–H$^{ip.bend}$	1011^m	1011	C–H$^{ip.bend}$
	1022	C–H$^{op.bend}$	1035^m	1020	C–H$^{op.bend}$
1088^w	1096	N-O$^{str.}$	1088^s	1085	N–O$^{str.}$
				1122	O–H$^{str.}$
	1286	N–H^{bend}	1305^m	1309	N–H^{bend}
1327^s	1355	CH$_3^{deformation}$			
1366^m	1371	C–C$^{str.}$			
1390^m	1410	OH^{bend}		1410	OH^{bend}
		C–N$^{op.bend}$			C–N$^{op.bend}$
	1507	C–N$^{str.}$	1495^m	1503	C–N$^{str.}$N–H^{bend}
1619^m	1667	C=O$^{str.}$	1600^s	1627	C=O$^{str.}$
2941^s	2945	C–H$^{as.str.}$		2967	O–H$^{str.}$
2998^m	3019	C–H$^{str.}$		3066	CH$_3^{deformation}$

Wavenumber is given in cm^{-1}

w weak, *m* medium, *s* strong, *as* asymmetric, *str.* stretching, *ip* in plane, *op* out plane, *bend* bending

In Fig. 8b, the peaks at 1011 and 1035 cm^{-1} represent C–H bending in plane and C–H bending out of plane. The bands with medium intensities at 1305 and 1495 cm^{-1} could be assigned to N–H bending and C-N stretching, while the strong bands at 1088 and 1600 cm^{-1} are from N–O stretching and C=O stretching. According to the surface selection rule for SERS [51, 52] and the SERS mechanism [53, 54], the enhanced bands in the SERS spectrum might correspond to either the vibrational moieties attached to the surface or the vibration direction perpendicular to the metal surface; in contrast, the intensities of vibrational modes with parallel polarized components to the surface will be decreased. Thus, the N–O and C=O groups might be perpendicular to the surface, due to their high SERS intensities. The proposed adsorption model of AHA at the copper surface is shown in Fig. 10.

Quantum chemistry calculations

As mentioned in SERS spectrum analysis, AHA molecule may adsorb at the copper surface by transferring electrons from the N–O and C=O groups to the unfilled hybrid orbital of copper; quantum chemical calculations are used to predict the feasible adsorption centers of a free single molecule on the bare metal surface to confirm the relationship between the AHA molecular structures and its inhibition property. In addition, note that all the calculated parameters obtained in the gas phase and the solvent effects were ignored.
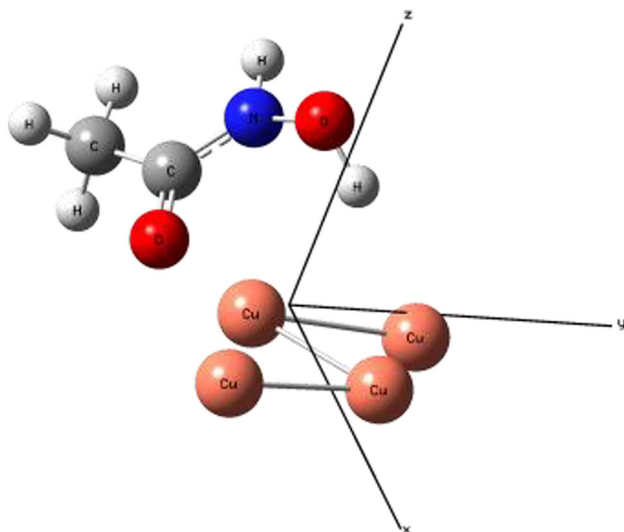
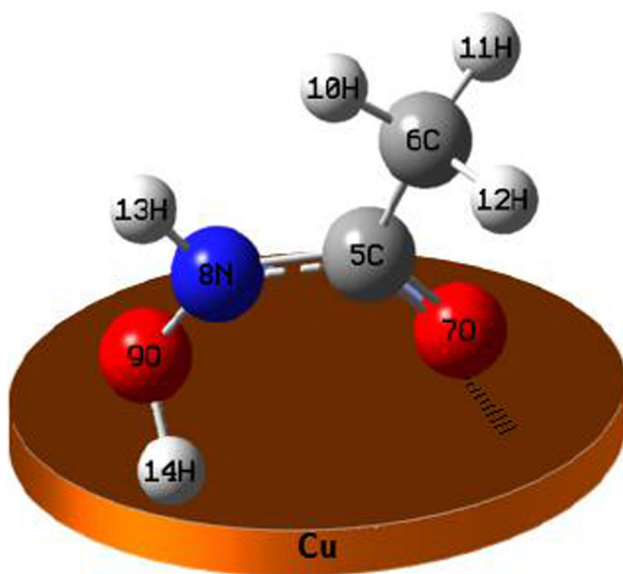**Fig. 9** The geometry model of AHA-Cu₄ optimized by B3LYP/LANI2DZ method

Fig. 10 The proposed adsorption model of AHA on the copper surface

Fig. 11 Molecular orbital plots for acetohydroxamic acid
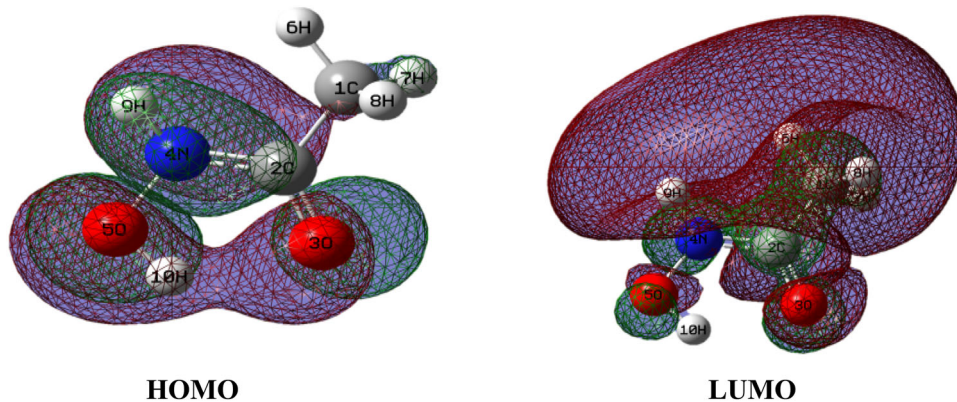

HOMO

LUMO

Table 8 Quantum chemical parameter comparison of some molecules in literature with the AHA molecule calculated with DFT method

	E_{LUMO} (kJ mol^{-1})	E_{HOMO} (kJ mol^{-1})	ΔE (kJ mol^{-1})	μ (Debye)
AHA	−175.9	−427.6	251.8	5.413
MPTT	−0.072	−0.186	0.114	9.834
AAP	−0.505	−5.296	4.791	4.257

The geometry of the AHA is fully optimized based on the method of B3LYP/LANI2DZ. The illustration of the highest occupied molecular orbital (HOMO) and the lowest unoccupied molecular orbital (LUMO) is given in Fig. 11. The quantum chemical parameters, such as E_{HOMO}, E_{LUMO}, dipole moment, μ, the energy gap, ΔE ($\Delta E = E_{LUMO} - E_{HOMO}$), are listed in Table 8.

Clearly in Table 8, the high value of E_{HOMO} ($E_{HOMO} = -427.64$ kJ mol^{-1}) indicates the strong ability of AHA molecule donating electrons to form covalent bond with unoccupied d-orbitals of metal [55], while the low value of E_{LUMO} ($E_{LUMO} = -175.86$ kJ mol^{-1}) indicates that the AHA molecule has a tendency to accept electrons from d-orbitals of metal to form back-donating bond. The values of the high dipole moment ($\mu = 5.4125$ D) and the low energy gap ($\Delta E = 251.78$ kJ mol^{-1}) facilitate adsorption to the copper surface and, therefore, enhance the inhibition efficiency [56], which is in good agreement with the experimental results.

It can be found in Fig. 11 that the HOMO is located within the region around the N–O and C=O groups, which could be regarded as the feasible sites for interaction with the copper surface. Additionally, the nitrogen atom and two oxygen atoms have large electron densities and their Mulliken atomic charges are −0.302, −0.357 and −0.363, respectively. Thus, AHA can adsorb on the copper surface by donating the electrons from the two O atoms to the d-orbitals of copper.

Conclusions

Consequently, the above investigations confirm that the application of acetohydroxamic acid as an effective corrosion inhibitor for copper in 3 wt% NaCl solution is promising. Some conclusions could be drawn:

1. A relatively compact AHA film could be formed on the copper surface in 10 mM AHA solution for 3 h assembly time and its inhibition efficiency in 3 wt% NaCl solution reached 93.5%, supported by surface morphologies images recorded when the copper with optimized AHA film corroded in 3 wt% NaCl solution for 5 h.
2. Adsorption of AHA on the copper surface fits Langmuir adsorption isotherm.
3. AHA molecules adopted the N–O and C=O groups to attach onto the surface for constructing the protection film.

References

1. Issaadi S, Douadi T, Chafa S (2014) Adsorption and inhibitive properties of a new heterocyclic furan Schiff base on corrosion of copper in HCl 1 M: experimental and theoretical investigation. Appl Surf Sci 316:582–589
2. Lei YH, Ohtsuka T, Sheng N (2015) Corrosion protection of copper by polypyrrole film studied by electrochemical impedance spectroscopy and the electrochemical quartz microbalance. Appl Surf Sci 357:1122–1132
3. Song P, Guo XY, Pan YC, Shen S, Sun YQ, Wen Y, Yang HF (2013) Insight in cysteamine adsorption behaviors on the copper surface by electrochemistry and Raman spectroscopy. Electrochim Acta 89:503–509
4. Tian H, Li W, Cao K, Hou B (2013) Potent inhibition of copper corrosion in neutral chloride media by novel non-toxic thiadiazole derivatives. Corros Sci 73:281–291
5. Zhang DQ, Gao LX, Zhou GD (2004) Inhibition of copper corrosion by bis-(1-benzotriazolymethylene)-(2,5-thiadiazoly)-disulfide in chloride media. Appl Surf Sci 225:287–293
6. Yu YZ, Zhang DQ, Zeng HJ, Xie B, Gao LX, Lin T (2015) Synergistic effects of sodium lauroyl sarcosinate and glutamic acid in inhibition assembly against copper corrosion in acidic solution. Appl Surf Sci 355:1229–1237
7. Tian HW, Cheng YF, Li WH, Hou BR (2015) Triazolyl-acyl-hydrazone derivatives as novel inhibitors for copper corrosion in chloride solutions. Corros Sci 100:341–352
8. Ghelichkhah Z, Sharifi-Asl S, Farhadi K, Banisaied S, Ahmadi S, Macdonald DD (2015) L-cysteine/polydopamine nanoparticle-coatings for copper corrosion protection. Corros Sci 91:129–139
9. Wang D, Xiang B, Liang YP, Song S, Liu C (2014) Corrosion control of copper in 3.5 wt% NaCl solution by domperidone: experimental and theoretical study. Corros Sci 85:77–86
10. Hegazy MA, Hasan AM, Emara MM, Bakr MF, Youssef AH (2012) Evaluating four synthesized Schiff bases as corrosion inhibitors on the carbon steel in 1 M hydrochloric acid. Corros Sci 65:67–76
11. Mahdavian M, Ashhari S (2010) Corrosion inhibition performance of 2-mercaptobenzimidazole and 2-mercaptobenzoxazole compounds for protection of mild steel in hydrochloric acid solution. Electrochim Acta 55:1720–1724
12. Avci G (2008) Corrosion inhibition of indole-3-acetic acid on mild steel in 0.5 M HCl. Colloids Surf A Physicochem Eng Asp 317:730–736
13. Ansari KR, Quraishi MA, Singh A (2014) Schiff's base of pyridyl substituted triazoles as new and effective corrosion inhibitors for mild steel in hydrochloric acid solution. Corros Sci 79:5–15
14. Behpour M, Mohammadi N (2012) Investigation of inhibition properties of aromatic thiol self-assembled monolayer for corrosion protection. Corros Sci 65:331–339
15. Lokesh KS, Keersmaecker MD, Elia A, Depla D, Dubruel P, Vandenabeele P, Vlierberghe SV, Adriaens A (2012) Adsorption of cobalt(II) 5,10,15,20-tetrakis(2-aminophenyl)-porphyrin onto copper substrates: characterization and impedance studies for corrosion inhibition. Corros Sci 62:73–82
16. Golestani Gh, Shahidi M, Ghazanfari D (2014) Electrochemical evaluation of antibacterial drugs as environment-friendly inhibitors for corrosion of carbon steel in HCl solution. Appl Surf Sci 308:347–362
17. Zhang DQ, Gao LX, Zhou GD (2005) Inhibition of copper corrosion in aerated hydrochloric acid solution by amino-acid compounds. J Appl Electrochem 35:1081–1085
18. Ramezanzadeh B, Vakili H, Amini R (2015) The effects of addition of poly(vinyl) alcohol (PVA) as a green corrosion inhibitor to the phosphate conversion coating on the anticorrosion and adhesion properties of the epoxy coating on the steel substrate. Appl Surf Sci 327:174–181
19. Yang HF, Feng J, Liu YL, Yang Y, Zhang ZR, Shen GL, Yu RQ (2004) Electrochemical and surface enhanced Raman scattering spectroelectrochemical study of phytic acid on the silver electrode. J Phys Chem B 108:17412–17417
20. Dost K, Tokul O (2006) Determination of phytic acid in wheat and wheat products by reverse phase high performance liquid chromatography. Anal Chim Acta 558:22–27
21. El-Sayed AR, Harm U, Mangold KM, Fürbeth W (2012) Protection of galvanized steel from corrosion in NaCl solution by coverage with phytic acid SAM modified with some cations and thiols. Corros Sci 55:339–350
22. Reddy AS, Kumar MS, Reddy GR (2000) A convenient method for the preparation of hydroxamic acids. Tetrahedron Lett 41:6285–6288
23. Farkas E, Enyedy ÉA, Csóka H (1999) A comparison between the chelating properties of some dihydroxamic acids, desferrioxamine B and acetohydroxamic acid. Polyhedron 18:2391–2398
24. Farkas E, Enyedy ÉA, Zekany L, Deak G (2001) Interaction between iron(II) and hydroxamic acids: oxidation of iron(II) to iron(III) by desferrioxamine B under anaerobic conditions. J Inorg Biochem 83:107–114
25. Alagta A, Felhösi I, Kálmán E (2007) Hydroxamic acid corrosion inhibitor for steel in aqueous solution. Mater Sci Forum 537–538:81–88

26. Ezznaydy G, Shaban A, Telegdi J, Ouaki B, Hajjaji SE (2015) Inhibition of copper corrosion in saline solution by mono-hydroxamic acid. J Mater Environ Sci 6(7):1819–1823

27. Telegdi J, Rigó T, Kálmán E (2005) Molecular layers of hydroxamic acids in copper corrosion inhibition. J Electroanal Chem 582:191–201

28. Brown GM, Hope GA (1995) In-situ spectroscopic evidence for the adsorption of SO_4^{2-} ions at a copper electrode in sulfuric acid solution. J Electroanal Chem 382:179–182

29. Gao X, Zhao CC, Lu HF, Gao F, Ma H (2014) Influence of phytic acid on the corrosion behavior of iron under acidic and neutral conditions. Electrochim Acta 150:188–196

30. Hong S, Chen W, Luo HQ, Li NB (2012) Inhibition effect of 4-amino-antipyrine on the corrosion of copper in 3 wt% NaCl solution. Corros Sci 57:270–278

31. Pan YC, Wen Y, Xue LY, Guo XY, Yang HF (2012) Adsorption behavior of methimazole monolayers on a copper surface and its corrosion inhibition. J Phys Chem C 116:3532–3538

32. Hong S, Chen W, Zhang Y, Luo HQ, Li M, Li NB (2013) Investigation of the inhibition effect of trithiocyanuric acid on corrosion of copper in 3.0 wt% NaCl. Corros Sci 66:308–314

33. Reznik VS, Akamsin VD, Khodyrev YP, Galiakberov RM, Efremov YY, Tiwari L (2008) Mercaptopyrimidines as inhibitors of carbon dioxide corrosion of iron. Corros Sci 50:392–403

34. Skale S, Doleček V, Slemnik M (2007) Substitution of the constant phase element by Warburg impedance for protective coatings. Corros Sci 49:1045–1055

35. Soltani N, Behpour M, Oguzie EE, Mahluji M, Ghasemzadeh MA (2015) Pyrimidine-2-thione derivatives as corrosion inhibitors for mild steel in acidic environments. RSC Adv 5:11145–11162

36. Li CC, Guo XY, Shen S, Song P, Xu T, Wen Y, Yang HF (2014) Adsorption and corrosion inhibition of phytic acid calcium on the copper surface in 3 wt% NaCl solution. Corros Sci 83:147–154

37. Sherif EM, Park SM (2006) Effects of 2-amino-5-ethylthio-1,3,4-thiadiazole on copper corrosion as a corrosion inhibitor in aerated acidic pickling solutions. Electrochim Acta 51:6556–6562

38. Pan YC, Wen Y, Guo XY, Song P, Shen S, Du YP, Yang HF (2013) 2-Amino-5-(4-pyridinyl)-1,3,4-thiadiazole monolayers on copper surface: observation of the relationship between its corrosion inhibition and adsorption structure. Corros Sci 73:274–280

39. Li W, Hu LC, Zhang SG, Hou BR (2011) Effects of two fungicides on the corrosion resistance of copper in 3.5% NaCl solution under various conditions. Corros Sci 53:735–745

40. Qin TT, Li J, Luo HQ, Li M, Li NB (2011) Corrosion inhibition of copper by 2,5-dimercapto-1,3,4-thiadiazole monolayer in acidic solution. Corros Sci 53:1072–1078

41. Scendo M (2007) The effect of purine on the corrosion of copper in chloride solutions. Corros Sci 49:373–390

42. Chen W, Hong S, Li HB, Luo HQ, Li M, Li NB (2012) Protection of copper corrosion in 0.5 M NaCl solution by modification of

5-mercapto-3-phenyl-1,3,4-thiadiazole-2-thione potassium self-assembled monolayer. Corros Sci 61:53–62

43. Zhang F, Tang YM, Cao Z, Jing WH, Wu ZL, Chen YZ (2012) Performance and theoretical study on corrosion inhibition of 2-(4-pyridyl)-benzimidazole for mild steel in hydrochloric acid. Corros Sci 61:1–9

44. Zhou X, Yang HY, Wang FH (2011) [BMIM] BF4 ionic liquids as effective inhibitor for carbon steel in alkaline chloride solution. Electrochem Acta 56:4268–4275

45. Abd El Rehim SS, Sayyah SM, El-Deeb MM, Kamal SM, Azooz RE (2016) Adsorption and corrosion inhibitive properties of P(2-aminobenzothiazole) on mild steel in hydrochloric acid media. Int J Ind Chem 7:39–52

46. Benahmed M, Djeddi N, Akkal S, Laouar H (2016) Saccocalyx satureioides as corrosion inhibitor for carbon steel in acid solution. Int J Ind Chem 7:109–120

47. Madkour LH, Elshamy IH (2016) Experimental and computational studies on the inhibition performances of benzimidazole and its derivatives for the corrosion of copper in nitric acid. Int J Ind Chem 7:195–221

48. Morad MS (2008) Corrosion inhibition of mild steel in sulfamic acid solution by S-containing amino acids. J Appl Electrochem 38:1509–1518

49. Tao S, Yu LJ, Pang R, Huang YF, Wu DY, Tian ZQ (2013) Binding interaction and Raman spectra of p–π conjugated molecules containing CH_2/NH_2 groups adsorbed on silver surfaces: a DFT study of wagging modes. J Phys Chem C 117:18891–18903

50. Shen S, Guo XY, Song P, Pan YC, Wang HQ, Wen Y, Yang HF (2013) Phytic acid adsorption on the copper surface: observation of electrochemistry and Raman spectroscopy. Appl Surf Sci 276:167–173

51. Moskovits M (1982) Surface selection rules. J Chem Phys 77:4408–4416

52. Moskovits M, Suh JS (1984) Surface selection rules for surface-enhanced Raman spectroscopy: calculations and application to the surface-enhanced Raman spectrum of phthalazine on silver. J Phys Chem 88:5526–5530

53. Félidj N, Aubard J, Lévi G, Krenn JR, Salerno M, Schider G, Lamprecht B, Leitner A, Aussenegg FR (2002) Controlling the optical response of regular arrays of gold particles for surface-enhanced Raman scattering. Phys Rev B 65:075419

54. McFarland AD, Young MA, Dieringer JA, VanDuyne RP (2005) Wavelength-scanned surface-enhanced Raman excitation spectroscopy. J Phys Chem B 109:11279–11285

55. Akalezi CO, Oguzie EE (2016) Evaluation of anticorrosion properties of Chrysophyllum albidum leaves extract for mild steel protection in acidic media. Int J Ind Chem 7:81–92

56. Yan Y, Li WH, Cai LK, Hou BR (2008) Electrochemical and quantum chemical study of purines as corrosion inhibitors for mild steel in 1 M HCl solution. Electrochem Acta 53:5953–5960